particle motion between sites in the vicinity of the defect rather than direct absorption by band electrons. The anisotropy of the changes in attenuation indicate the particle sites are well defined. Only modes associated with the C_{44} elastic constant are effected by the reduction, suggesting that the motion is between sites which became inequivalent as a result of the strain associated with the C_{44} elastic constant.

ACKNOWLEDGMENTS

Computer Studies in Self-Focusing*

E. L. Dawes† and J. H. Marburger
University of Southern California, Los Angeles, California 90007
(Received 8 November 1968)

We report extensive numerical solutions of the electromagnetic wave equation with a saturable, complex, intensity-dependent refractive index. The "large-scale" self-focusing region is fully explored, and some aspects of "small-scale" self-trapping induced by saturation of the nonlinear index are investigated. We find that many features of the numerical solutions are predicted rather well by the paraxial-ray–constant-shape approximation.

1. INTRODUCTION

THE phenomenon of self-focusing of intense optical beams in liquids with intensity-dependent refractive indices is of central importance in determining the nonlinear optical properties of these materials. Unfortunately, it is difficult to construct a theory of self-focusing which includes all the physical mechanisms which are known to influence the local optical intensity. In addition to processes such as orientational and translational molecular redistribution which give rise to the nonlinear refractive index itself, one must also include in a proper theory such inelastic processes as stimulated Raman and Brillouin scattering. Moreover, comparison of any such theory with experiment is awkward because of the uncertainty in the spatial and temporal properties of the primary laser radiation.

In view of this complexity there seems to be some advantage in studying each part of the self-focusing problem separately in depth before attempting a comprehensive theory. We report in this paper the results of one such study in which all time-dependent and inelastic scattering processes are ignored. The entire response of the nonlinear medium is assumed to be contained in an intensity-dependent complex refractive index. This leads to an approximate nonlinear wave equation for the optical electric field which was first derived and solved numerically by Kelley[1] for a simple intensity-dependent index. Our work is a direct generalization of Kelley's.

After this study was completed, we discovered that very similar numerical results were reported by Goldberg, Talanov, and Erm (GTE) in Ref. 2, which is not yet available in English translation. While the program of GTE is remarkably like ours, we feel that sufficient differences exist in emphasis, domain of solution, and conclusions to justify publication of our results. Wherever possible, we have taken pains to compare our conclusions with those of GTE. Kelley[3] has also obtained numerical solutions similar to some of those reported here.

In Sec. 2 we present solutions of Kelley's original equation with neither absorption nor saturation of the nonlinear index. From these it is possible to determine the regions of validity of the various approximate analytical solutions of this equation, and to find the "dynamical critical power" for self-focusing. Similar results are given in Sec. 3 for a linearly absorbing medium. Here we analyze the relevant experiment of Kaiser et al.[4] and describe another which would be easier to compare with the theory. Section 4 includes our results for a saturable nonlinear index. In this case qualitatively new phenomena appear: the dynamical formation of rings in the transverse intensity distribution.[5] The inclusion of nonlinear absorption, discussed in Sec. 5, does not lead to significant or unexpected modifications of the previous results. Extreme care was taken to eliminate instabilities in the computing scheme as described in Sec. 6.

[1] P. L. Kelley, Phys. Rev. Letters 15, 1005 (1965).

[2] V. N. Goldberg, V. I. Talanov, and R. E. Erm, Izv. Vysshikh Uchebn. Zavedenii Radiofiz. 10, 674 (1967).
[3] P. L. Kelley (private communication).
[4] W. Kaiser, A. Laubereau, M. Maier, and J. A. Giordmaine, Phys. Letters 22, 60 (1966).
[5] J. H. Marburger and E. L. Dawes, Phys. Rev. Letters 21, 556 (1968).

In our attempts to understand the structure of our numerical solutions, we found the approximate analytical approach described by Wagner et al.[6] (WHM) to be most fruitful. The notation (WHM-3) means Eq. (3) in this reference. Other authors have used the paraxial-ray approximation employed in WHM, as cited there, but most of the results of this approach are summarized in WHM and for convenience we shall refer only to this work.

2. SIMPLEST NONLINEAR SUSCEPTIBILITY

The nonlinear equation whose solutions are analyzed in this section is simply Kelly's Eq. (9) [1]

$$i\partial E^*/\partial Z^* + \partial^2 E^*/\partial r^{*2}$$
$$+ r^{*-1}\partial E^*/\partial r^* + |E^*|^2 E^* = 0, \quad (2.1)$$

where $Z^* = Z/2ka^2$, $r^* = r/a$, $E^* = (\epsilon_2/2\epsilon_0)^{1/2} kaE$, and a is the variance of the Gaussian transverse optical field distribution that we assume at longitudinal distance $z=0$. E is the peak electric field amplitude, k is the wave number in the medium, and ϵ_2 is the nonlinear dielectric constant employed by Chiao et al.[7] This expression follows from the wave equation of electromagnetic theory if the divergence of $\mathbf{E}$ is ignored along with the second derivative of the slowly varying amplitude $E(r,z)$ with respect to z. Also neglected are inelastic scattering (frequency-shifting) processes. The constitutive equation which must be used to obtain (2.1) is

$$D = \epsilon_0 E + \epsilon_2 \langle |E|^2 \rangle_{av} E, \quad (2.2)$$

where $\langle \rangle_{av}$ denotes a time average over many cycles. For more detailed discussion of the approximations involved in deriving (2.1), see Refs. 1 and 6.

Since Eq. (2.1) has no free parameters, its solutions may be classified according to the properties of the initial values for the field at $z=0$. Throughout this paper we restrict ourselves to equiphase cylindrically symmetrical initial field distributions with a single maximum at $r=0$. Except where noted, the field distribution is Gaussian with variance a: $E = E_0 e^{-r^2/2a^2}$.

In Fig. 1 we have plotted a set of curves obtained from numerical solutions of (2.1) showing the on-axis intensity $(r=0)$ versus z for a number of powers in the input beam relative to the "dynamical critical power" P_2 for self-focusing. The criterion for determining P_2 is evident: For beam powers $P > P_2$ the on-axis intensity is "unbounded" for some $z=z_f$, where z_f is the "self-focusing length."[1] This critical power should be compared with P_{CGT} obtained by Chiao et al.[7] (CGT) in the solution of the ordinary differential equation describing the propagation of a beam whose transverse shape does not change with z. We find that for a Gaussian input $(P_2 - P_{CGT})/P_2 = 0.013$. Thus we may take $P_2 \approx P_{CGT}$.

[6] W. G. Wagner, H. A. Haus, and J. H. Marburger, Phys. Rev. 175, 256 (1968).

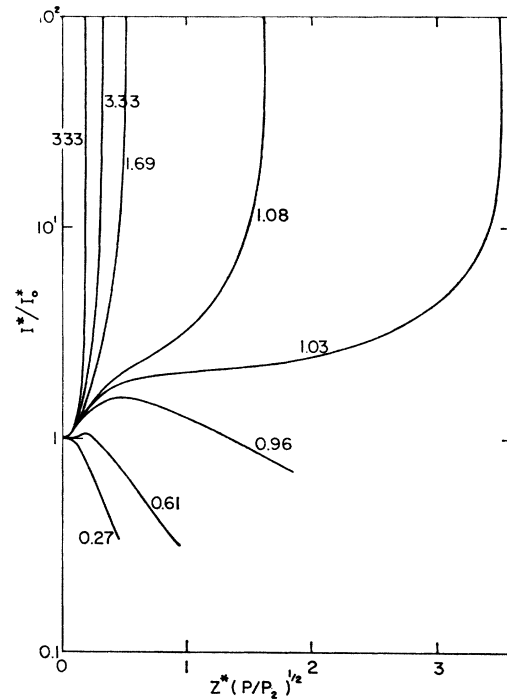[7] R. Y. Chiao, E. Garmire, and C. H. Townes, Phys. Rev. Letters 13, 479 (1964).

FIG. 1. Normalized on-axis intensity I^*/I_0^* versus axial distance in units of the near-field length $2ka_0^2 \times (P/P_2)^{-1/2}$. Curves are parametrized by P/P_2.

This result was also obtained by GTE. With our definition of ϵ_2,

$$P_2 = (1.22\lambda_0)^2 c\epsilon_0^{1/2}/64\epsilon_2,$$

where $\lambda_0 = 2\pi\epsilon_0^{1/2} k^{-1}$.

The paraxial-ray analysis of Talanov (see WHM) predicts a critical power $P_1 = 0.273 P_2$. Our numerical solutions show that for $P_1 < P < P_2$ the on-axis intensity rises initially to a "weak" focus and then falls to zero as if the beam were diffracting. This behavior can be understood from an examination of Eq. (WHM-2.10) for Gaussian beams with powers in this region. This equation, which is the equation of motion for a ray, shows that rays near the axis experience a net focusing force, while the periphery of the beam feels a net diffractive force. Thus the on-axis intensity always increases initially for $P > P_1$. GTE show plots of ray trajectories for $P_1 < P < P_2$ and $P_2 < P$ which display this behavior. This argument also shows that the radial intensity profile becomes peaked on axis, but with very wide wings, a feature of the CGT stationary profile.[7] In fact, we find that in the flat portion of curves such as that in Fig. 1, for which $P/P_2 = 1.03$, the radial profile is very close to the CGT shape.

From the data of Fig. 1 it is easy to find the dependence of the self-focusing length on the input power. Figure 2 shows that Z_f^{-1} is asymptotically a linear function of $P^{1/2}$, the equation for the asymptote being

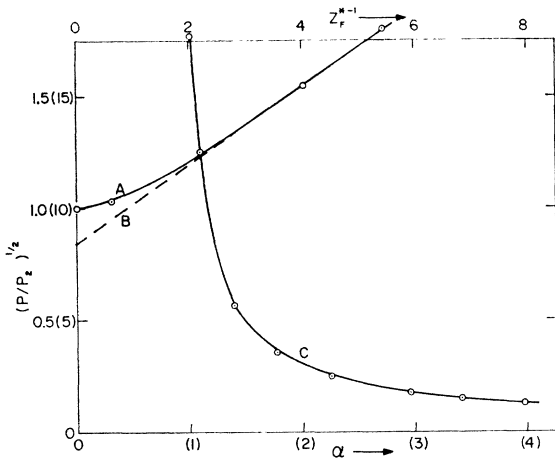$$(P/P_2)^{1/2} = 0.858 + 0.369 ka^2 Z_f^{-1}. \quad (2.3)$$

FIG. 2. P_2 versus inverse self-focusing length. A, square root of ratio of input power to critical power; B, asymptote of A for high powers; C, square root of ratio of input power to critical power versus parameter α appearing in Eq. (2.4). Note that two different ordinate scales are used. The nonparenthetic scale refers to A and B, the parenthetic scale to C.

This formula may be used to determine the critical power from measurements of the self-focusing length versus power. We stress that the numerical constants in (2.3) are valid only for Gaussian input beams. (Other shapes are discussed below.) Wang's[8] experimental determinations of P_2 by this method employ an approximate formula of Kelley's[1] in which the constant $c=0.858$ is replaced by unity. This leads to an underestimate of the actual critical power.

GTE also obtain a curve such as A in Fig. 2 and fit it with a hyperbola whose asymptote (in our notation) is given by (2.3) with slope 0.366 and intercept 0.824. The small discrepancy in slope may be attributed to GTE's use of solutions with P not exceeding $54P_2$, while our maximum power was $333P_2$. Therefore our determination of the asymptote is more accurate.

When comparing the results of GTE with ours, one must bear in mind that in GTE the width b of the input Gaussian, rather than the power, is used as a parameter. A change in b, with fixed input on-axis intensity, changes the input power as well as the beam diameter. Our use of the input power as a parameter with fixed beam width allows the curves of Fig. 1 to be compared directly with experiments in which, for example, the input power changes with time, but not the beam radius.

For $P/P_2 \gtrsim 1.5$, the following analytical formula is a fairly good representation of the curves in Fig. 1:

$$I(z)/I(0) = [1-(z/z_f)^2]^{-\alpha/2}, \quad P>1.5P_2 \quad (2.4)$$

where α is a parameter which depends on power as shown in Fig. 2. For $P/P_2 \gtrsim 100$, α is approximately unity, so that (2.4) reduces to the formula proposed by Kelley.[1] We find that Kelley's numerical curve,[1] with $z_f^* \approx 0.01$, corresponds to $P/P_2 \approx 333$.

[8] C. C. Wang, Phys. Rev. Letters **16**, 344 (1966).

At low power $P \lesssim 0.25P_2$, the formula (WHM-3.7) predicted by the paraxial-ray approximation fits the numerical solution well:

$$I(z)/I(0) = \{1+[1-(P/P_2)](z/ka^2)^2\}^{-1},$$
$$P \lesssim 0.25P_2. \quad (2.5)$$

For input beams whose transverse shapes are not Gaussian, but still smooth and with a single maximum, we find that the "f factor" is a useful concept. Defining a beam radius a_R by

$$a_R^2 = 2 \int_0^\infty g^2(r) r \, dr,$$

where the input field distribution is $E(r) = E_{max} g(r)$, and a transverse radius of curvature a_T by $g^2(r) = 1-(r/a_T)^2+\cdots$, we define $f \equiv a_R/a_T$. With this definition we have found numerically that for all smooth non-Gaussian beams that we used as inputs, (2.3) becomes

$$(P/P_2)^{1/2} \approx 0.369 ka_R^2(fz_f)^{-1}$$

for $P \gg P_2$. This agrees with a formula suggested by Wang.[8] We have also found that the dynamical critical power for self-focusing for beams with $f \neq 1$ increases as f increases.

3. EFFECTS OF LINEAR ABSORPTION

Numerical solutions of (2.1) with the additional term $\frac{1}{2}i\gamma^* E^*$ added to the left-hand side were obtained for a variety of situations. Figure 3 shows a family of on-axis
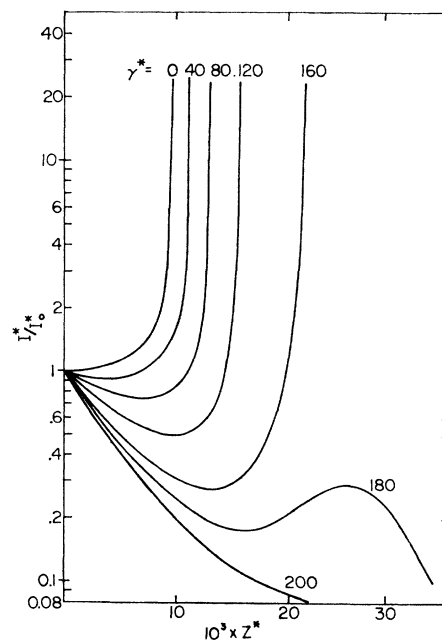

FIG. 3. Normalized on-axis intensity I^*/I_0^* versus axial distance in units of the near-field length $2ka_0^2$. Curves are parametrized by the linear absorption coefficient. Input power $P = 333P_2$.
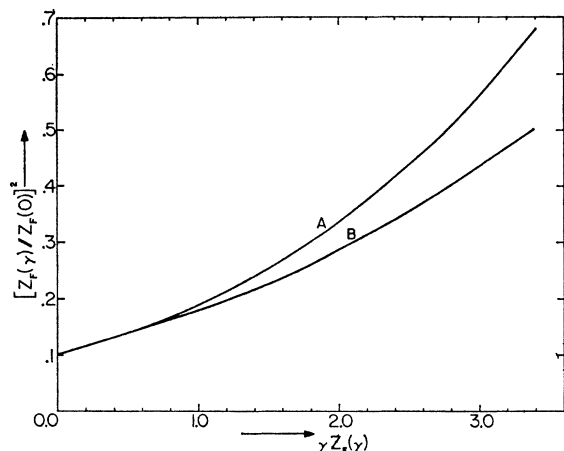
FIG. 4. Square of ratio of self-focusing length with linear absorption to self-focusing length without linear absorption versus product of linear absorption coefficient and self-focusing length. Input power $P = 333P_2$. A, Eq. (3.1); B, computer results.

intensity versus z^* curves obtained from these solutions, each curve corresponding to the same input power $P = 333P_2$ but a different absorption coefficient γ^*. The parameter γ^* is related to the usual absorption coefficient γ via

$$\gamma^* = 2ka^2\gamma.$$

A similar family of curves was obtained by GTE for $P = 13.4P_2$, with $0 \leq \gamma^* \leq 20$, and shows exactly the same qualitative behavior. In particular, there is a catastropic focus only for sufficiently small absorption, $\gamma^* < \gamma_{max}^* (P/P_2)$. From our solutions, $\gamma_{max}^* (333) \approx 170$, and from GTE, $\gamma_{max}^* (13.4) \approx 16$. This behavior is not at all surprising: If the self-focusing length exceeds somewhat the absorption length, too much power will be lost to allow a sharp focus. Thus γ_{max}^* should be proportional to z_f^{-1} and therefore, for sufficiently large powers, to $(P/P_2)^{1/2}$. This is roughly consistent with the numbers cited above.

Using an equation derived by Kaiser et al. [Eq. (3) of Ref. 4] which is based upon the paraxial-ray formalism, it is possible to find an approximate formula for the curves in Fig. 3:

$$I/I_0 = e^{-\gamma^* z^*}\{1 - (58.6P/P_2\gamma^{*2})$$
$$\times [1 - e^{-\gamma^* z^*}(1 + \gamma^* z^*)]\}^{-1/2}. \quad (3.1)$$

When the bracketed quantity in (3.1) approaches zero, the intensity increases without bound. Experimentally one may fix the cell length z and vary γ and P to achieve a focus near the cell exit, as in the experiment of Kaiser et al.[4] In this case one always has a catastrophic focus and γ never exceeds γ_{max}. Alternatively, one could fix P and vary γ and z to achieve a focus and in this way determine γ_{max} experimentally. Since this experiment probes the region of "anomalous" curves in Fig. 3, one may expect the approximate Eq. (3.1) to be inaccurate. Figure 4 compares the predictions of (3.1) for this

experiment with our numerical results. Here $z_f(\gamma)/z_f(0)$ is the ratio of the self-focusing length with absorption to that without absorption at fixed input power. Both curves stop when $\gamma = \gamma_{max}$.

4. SATURABLE NONLINEAR SUSCEPTIBILITY

The most important properties of the solutions of Eq. (2.1) with the final term replaced by $|E^*|^2 E^*/(1 + |E^*/E_s^*|^2)$ have been reported in Ref. 5, but here, for completeness, we shall repeat some of the arguments of that letter. Our aim in studying the effects of saturation of the nonlinear refractive index is not so much to obtain a single numerical solution of an equation in which all the parameters have realistic values, but rather to determine how the structure of the solution depends upon these parameters. In fact, we believe that the microscopic theory of the nonlinear index is not yet sufficiently well developed to yield realistic values of the parameter E_s^* even to within orders of magnitude.

The approximate analysis of WHM indicates that saturation of the index prevents a catastrophic focus: At the focus, there is a maximum intensity and a corresponding minimum beam radius. Moreover, the focus itself occurs at a somewhat larger axial distance than for no saturation. Beyond the first focus the beam diffracts out to its original radius, whereupon the "self-focusing force" takes over and the process repeats itself, giving rise to a series of foci spaced $2Z_f$.

Our numerical results indicate that these conclusions are correct as long as the constant-shape assumption of WHM is not violated. For example, in Fig. 5, we show the prediction of (WHM-3.19) for the ratio of the self-focusing length for a saturable index to that without saturation as a function of the saturation intensity $I_s^* \equiv E_s^{*2}$ (dashed line). The solid line is plotted from our numerical solutions and is in fair agreement with the approximate theory. Here the beam power was taken to be rather high: $P \equiv 333P_2$. For lower powers,
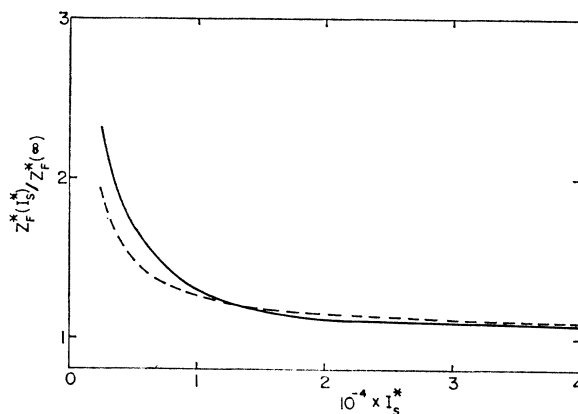

FIG. 5. Ratio of self-focusing length with saturation to that without saturation as a function of the saturation field $I_s^* = E_s^{*2}$. Input power $P = 333P_2$. Computer result, solid curve; Eq. (WHM-3.19), dashed line.
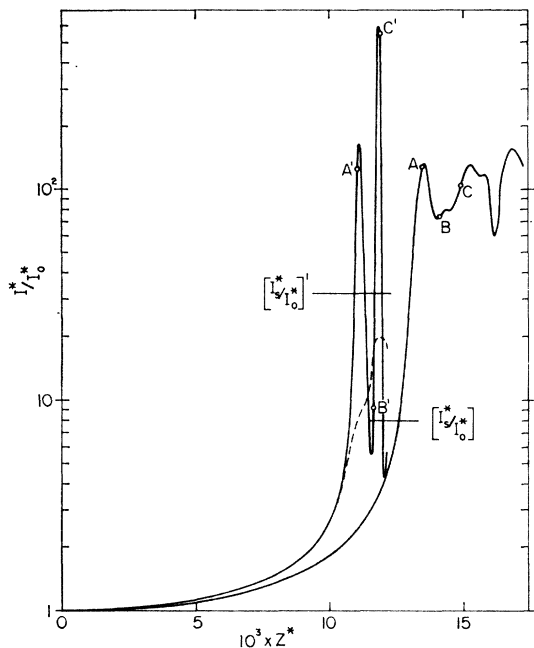
Fig. 6. Normalized on-axis intensity versus axial distance in units of the near-field length $2ka_0^2$. ABC, $I_s^* = 10\,000$; A'B'C', $I_s^* = 40\,000$. Input power $P = 333P_2$. Dashed line is normalized intensity averaged over a small radial region versus axial distance for $I_s^* = 40\,000$.

the approximate reduction in Z_f may be inferred from (WHM-3.19) or from Fig. 4 of WHM.

Figure 6, which shows normalized on-axis intensities versus Z^* for two different saturation fields (solid curves) obtained from our numerical solutions, con-
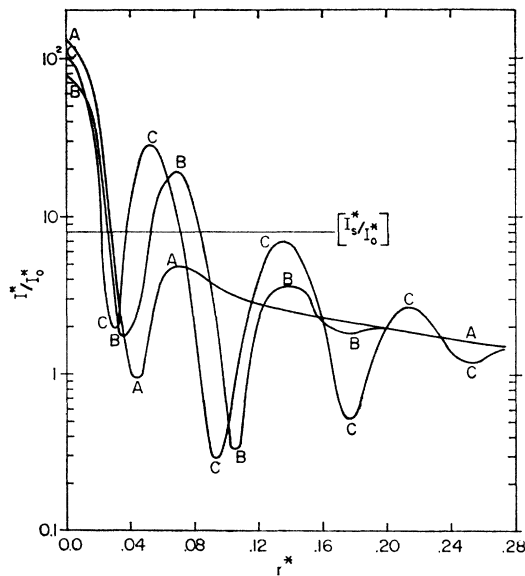

Fig. 7. Normalized intensity versus radial distance in units of the input radius a_0, taken at various axial positions ABC shown in Fig. 6.

firms the existence of a finite maximum at the focus. However, the subsequent behavior of the intensity is not at all that predicted by the paraxial-ray–constant-shape theory of WHM. The radial intensity profiles beyond the focus, shown in Figs. 7 and 8, show why: The constant-shape assumption is dramatically violated here. The formation of the radial rings shown in these figures comes about as follows: As the beam propagates, the refractive index near the axis rises at first but then becomes constant upon saturation. The resultant induced "convex lens" is flat in the center and therefore tends to focus incoming (still nearly parallel) rays into a ring. The rays initially bent toward the axis continue inward and give rise to a central maximum. The intensity in the ring also rises until a new "flat" region is
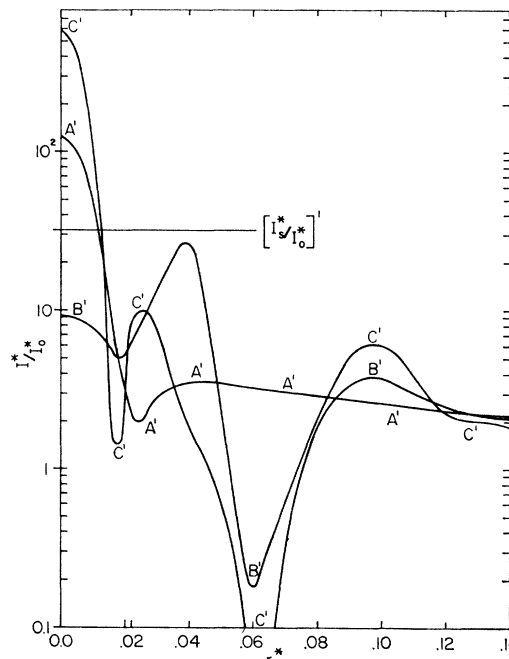

Fig. 8. Normalized intensity versus radial distance in units of the input radius a_0, taken at various axial positions A'B'C' shown in Fig. 6.

formed in the induced lens, whereupon a new ring begins to form.

Before discussing our numerical results in detail, it is of interest to compare the range of parameters for which we have solutions with that of GTE. These authors show on-axis intensity versus Z curves for beam power and saturation intensities $(P/P_2,\ I_s^*) = (1.21,\ 18)$, $(3.35,\ 50)$, $(13.4,\ 200)$. In contrast, we have solutions for $P/P_2 = 333$ and I_s^* ranging from 2500 to 40 000 (see Fig. 5), as well as a single solution with $P/P_2 = 33$ and $I_s^* = 10\,000$. For CS_2, P_2 is about 10 kW (for $\lambda_0 = 0.7\ \mu$) and the power for which most of our solutions have been obtained is about 3 MW, a power level easily achieved with modern Q-switched lasers. Realistic values of E_s^* are difficult to estimate in the absence of

any realistic theory of the saturation of the nonlinear index. A crude theory which treats the liquid as a gas of anisotropic molecules with mutual interactions represented only by Lorentz local field[6] yields roughly $E_s^* \approx 10^4$. This is nearly two orders of magnitude greater than that for which we have solutions, and three orders of magnitude greater than that for which GTE have solutions.

Complicated as the curves in Figs. 6–8 appear, their structure may be largely understood with the help of the results of the paraxial-ray analysis. The solutions with the lower saturation field, ABC in Figs. 6 and 7, are simplest and show that after the ring structure has formed, the central peak persists and oscillates weakly in intensity. The radius of this peak and of the first ring, measured to the point at which the intensity has diminished by $1/e$, are 0.019 and 0.086, respectively. For comparison, the minimum radius a_m^* and the equilibrium radius a_c^* predicted by the paraxial-ray theory for a Gaussian beam of power $P/P_2 = 333$ are 0.021 and 0.085, respectively. Fitting the central peak with a Gaussian and treating it as if the rings were absent, we find from (WHM-3.14) a period of oscillation $Z_*^* \approx 3 \times 10^{-3}$, which compares favorably with the distance $\approx 2 \times 10^{-3}$ between the two minima in the curve ABC in Fig. 6. The power in the central peak is about an order of magnitude greater than P_2 at the focus and decreases slowly at greater distances.

In contrast, the power in the central peak of the radial profiles plotted in Fig. 8 is not at all constant. Its fluctuations are reflected in the violent oscillations of the on-axis intensity as shown in Fig. 6, curve A'B'C'. However, the power in the central maximum *and* the first ring varies much less rapidly and exceeds P_2 by about an order of magnitude. The intensity averaged over a small area including the first ring is shown as a dashed line in Fig. 6.

The radius of the first ring, $r^* \approx 0.045$, is again close to the equilibrium radius predicted by the paraxial-ray theory, $a_c^* = 0.043$, and the corresponding predicted minimum radius $a_m^* = 0.01$ is close to the variance of the best Gaussian fit to the central peak of curve A' in Fig. 8, $r^* = 0.009$. The period of oscillation predicted by (WHM-3.14) for this Gaussian as an input beam is $Z_*^* = 0.80 \times 10^{-3}$, which agrees well with the numerical value 0.74×10^{-3} inferred from curve A'B'C' in Fig. 6.

The periodic transfer of power between the central peak and the first ring also occurs in our numerical solution for $P = 33P_2$, and here too the radial scale and period of oscillation of the on-axis intensity is given quite well by the paraxial-ray formulas.

This persistence of a very high intensity beyond the focus in a region very near the axis is strikingly similar to the observed "small-scale filament" formation ob-

served experimentally.[9-12] All of our numerical solutions of the self-focusing equation with saturable nonlinear index display this behavior, and in every case the transverse scale of the central region in which power is approximately conserved is in good agreement with the equilibrium radius a_c predicted by the paraxial-ray theory (WHM-3.12):

$$\frac{a_c}{a} = 1.91 \frac{(P/P_2)^{1/2}}{E_s^* [(P/P_2)^{1/2} - 1]^{1/2}}.$$

This is a weak function of P/P_2 for large powers and, for these, a_c will be practically independent of the properties of the input beam, in accord with the observations on small-scale filaments.[13] The actual magnitude of a_c depends upon the saturation properties of the nonlinear index and, for the particular model of the Kerr effect described in WHM, agrees well with the half-width of the stationary-shape solutions obtained in Refs. 14–16.

We emphasize that experimental observations of filament properties are invariably *time-averaged* over the duration of the input pulse. Quantitative comparison of theory with experiment will only be possible with the advent of a theory which includes time-dependent effects such as relaxation of the nonlinear polarization and stimulated inelastic scattering.

5. NONLINEAR ABSORPTION

A crude estimate of the effects of stimulated inelastic scattering on the stationary self-focusing process may be obtained by solving Eq. (2.1) with saturation and with an additional nonlinear absorption term $i\gamma^{*NL} |E^*|^2$. Such a term has been used by Giordmaine and Howe[17] to fit high-power transmission data in CS_2, which were subsequently shown by Maier et al.[18] to arise from backward stimulated Brillouin scattering.

Using the approach described in WHM, it is not difficult to derive the following set of approximate ordinary equations for the power and beam radius as a

[9] P. Lallemand and N. Bloembergen, Phys. Rev. Letters **15**, 1010 (1965).

[10] E. Garmire, R. Y. Chiao, and C. H. Townes, Phys. Rev. Letters **16**, 347 (1966).

[11] R. Y. Chiao, M. A. Johnson, S. Krinsky, H. A. Smith, C. H. Townes, and E. Garmire, IEEE J. Quantum Electron. **2**, 467 (1966).

[12] R. G. Brewer and J. R. Lifsitz, Phys. Letters **23**, 79 (1966).

[13] Y. R. Shen and Y. J. Shaham, Phys. Rev. **163**, 224 (1967).

[14] J. D. Reichert and W. G. Wagner, IEEE J. Quantum Electron. **4**, 221 (1968).

[15] T. K. Gustafson, P. L. Kelley, R. Y. Chiao, and R. G. Brewer, Appl. Phys. Letters **12**, 165 (1968).

[16] J. H. Marburger, L. Huff, J. D. Reichert, and W. G. Wagner (unpublished).

[17] J. A. Giordmaine and J. A. Howe, Phys. Rev. Letters **11**, 207 (1963).

[18] M. Maier, W. Rother, and W. Kaiser, Phys. Letters **23**, 83 (1966).

function of z:

$$k^2 a^3 \frac{d^2 a}{dz^2} = 1 - \frac{P}{P_1}\left(1 + \frac{8P}{\epsilon_0^{1/2} c E_s^2 a^2}\right)^{-2}, \quad (5.1)$$

$$\frac{dP}{dz} = -\gamma P - \frac{\gamma^{*NL} P^2}{2k P_1 a^2}, \quad (5.2)$$

where

$$\gamma^{*NL} = \mathrm{Im}\epsilon_2 / \mathrm{Re}\epsilon_2.$$

Numerical solutions of these equations for $E_s = \infty$ (no saturation) and $\gamma = 0$ (no linear absorption) yield on-axis intensity versus z curves very similar in appearance to those shown in Fig. 3 for linear absorption. In particular, for each input power there is a maximum value of γ^{NL} above which a catastrophic focus does not take place. This critical nonlinear absorption coefficient γ_{max}^{*NL} was found to depend weakly on the input power:

$$\gamma_{max}^{*NL} \approx 0.16\{[1 + 2\ln(P/P_1)]^{1/2} - 1\}.$$

We emphasize that this result was *not* obtained by integration of Kelley's equation but of the approximate system, Eqs. (5.1) and (5.2).

Because of the crudeness of the nonlinear-absorption approach to the analysis of the effects of stimulated scattering phenomena, we were unwilling to lavish much computer time on solutions of Kelley's equation for this case. Consequently, insufficient solutions were obtained to determine the functional dependence of their structure on the additional parameter γ^{*NL}. Using $\gamma^{*NL} = 0.01$, which is consistent with the results of Giordmaine and Howe,[17] and the presumably low saturation fields $E_s^* = 100$, 200, we found little departure in the transverse structure, even near the focus, from that obtained with $\gamma^{*NL} = 0$. The axial distance between foci was somewhat larger than for $\gamma^{*NL} = 0$, as expected.

However, these results are inconclusive, since if E_s^* is really much larger than the values we used, the beam in reality focuses to a smaller diameter before filament formation and the on-axis intensity consequently reaches higher values. This would cause appreciably more absorption for fixed γ^{*NL}.

Furthermore, "realistic" values of γ^{*NL} may be only remotely related to those inferred in Refs. 17 and 18, because in the work reported there the transverse mode structure was undetermined. Therefore it is possible that the observed removal of power from the primary beam took place, not in a single near-axis region, but in several regions corresponding to "hot spots" in the transverse intensity distribution. This would lead to an observed γ^{*NL} larger than that appropriate for our single-mode analysis.

6. NUMERICAL COMPUTATION SCHEME

Numerical solutions of the self-focusing equation (2.1) including saturation and nonlinear absorption were obtained by converting it to a difference equation

which was then solved by an "explicit" iteration scheme on a digital computer. An explicit scheme, rather than an unconditionally stable implicit scheme, was chosen because of the simplicity with which nonlinear terms are treated. Following Kelly,[1] we performed a stability analysis in the manner described by Harmuth[19] (cited in Ref. 1) and found that the following scheme ensured negative error growth rates. Replace $\partial E^*/\partial Z^*$ by the two-point symmetric difference quotient, and the radial derivatives by symmetric five-point difference formulas. Setting $r^* = m\Delta r$ and $Z^* = n\Delta z$ with m and n integers, we found that the loss terms at the grid point (m,n) must be written

$$[\gamma^* E^*]_{m\Delta r, n\Delta z} = \tfrac{1}{2}\gamma^*[E_{m,n+1}^* + E_{m,n-1}^*],$$

$$[\gamma^{*NL} |E^*|^2 E^*]_{m\Delta r, n\Delta z}$$
$$= \tfrac{1}{2}\gamma^{*NL} |E^*|_{m,n}^2[E_{m,n+1}^* + E_{m,n-1}^*],$$

and, finally, that Δr and Δz must be related through

$$\Delta z < \left[\left(\frac{32/3}{(\Delta r)^2}\right)^2 + \left(\tfrac{1}{2}\gamma^* + \frac{\gamma^{*NL} 32/3}{(\Delta r)^2}\right)^2\right]^{-1/2}, \quad (6.1)$$

if

$$[F(E^*)]_{max} \le (32/3)/(\Delta r)^2$$

and

$$\Delta z < \{[F(E^*)]_{max}^2 + (\tfrac{1}{2}\gamma^* + \gamma^{*NL} |E^*|_{max}^2)^2\}^{-1/2},$$

if

$$[F(E^*)]_{max} > (32/3)/(\Delta r)^2,$$

where

$$F(E^*) \equiv \frac{|E^*|^2}{1 + |E^*|^2/E_s^{*2}}.$$

Here the subscript max means that the largest value attained should be used.

The first of these conditions on Δr and Δz is usually easier to satisfy and we have chosen it for all our computations. The second may be excluded if we require that $2\Delta r$ correspond to the wavelength of a transverse perturbation which is not amplified by the original differential equation. Using a linearized stability analysis exactly analogous to that of Bespalov and Talanov,[20] we find that such a perturbation will decay if

$$[F(E^*)]_{max} < \pi^2/(\Delta r)^2.$$

The relation (6.1) was well satisfied for all the computations reported here. The results reported in Secs. 4 and 5 were obtained using a CDC 6600 digital computer and the others were obtained with an IBM 360 model 40. In all cases for which absorption was absent the beam power remained constant to within 0.1%. Solutions obtained with different step sizes were consistent, but we did not test the effect of decreasing step size on every run.

[19] H. F. Harmuth, J. Math. Phys. **36**, 269 (1957).
[20] V. I. Bespalov and V. I. Talanov, Zh. Eksperim. i Teor. Fiz. Pis'ma v Redaktsiyu **3**, 471 (1966) [English transl.: Soviet Phys.—JETP Letters **3**, 307 (1966)].